Journal of Sound and Vibration (1997) **202**(2), 187–201

DYNAMIC ANALYSIS OF THE FLEXIBLE ROD OF A QUICK-RETURN MECHANISM WITH TIME-DEPENDENT COEFFICIENTS BY THE FINITE ELEMENT METHOD

R.-F. Fung and F.-Y. Lee

Department of Mechanical Engineering, Chung Yuan Christian University, Chung-Li, Taiwan 32023, *Republic of China*

(*Received* 18 *August* 1995, *and in final form* 15 *October* 1996)

The transient amplitude, dynamic stability and steady-state response of a flexible rod of a high-speed quick-return mechanism are investigated in this paper. The crank drives the rod by means of a translating/rotating joint at a constant speed. The flexible rod is divided into two regions. Each region has a time-dependent length and is modelled by the Timoshenko and Euler beam theories. A special finite element method with time-dependent shape and Hamilton's principle is employed to derive the governing equation, which has time-varying coefficients. By using the Runge–Kutta numerical method, the transient amplitudes are obtained. The steady-state responses due to harmonic excitation are determined by the harmonic balance method. Subsequently, Bolotin's method is used to solve Mathieu–Hill's type equation for the dynamic stability analysis. The stable–unstable boundaries are obtained from the condition that the set of linear homogeneous equations should have a non-trivial solution.

1. INTRODUCTION

Traditionally, mechanisms have been designed under the assumption that all members in a mechanism are rigid bodies. However, when a mechanism operates at a high-speed condition, a perturbative motion will be observed. There will be some problems in mechanism when the amplitude of vibration is greater than the allowable limit. Due to development of high-speed machinery, robots, and aerospace structures, research on the flexible systems undergoing both gross motion and elastic deformation has become increasingly important.

There are two general approaches in flexible mechanism analysis. These techniques are: (i) the coupled non-linear partial differential equations are generated analytically, and then Galerkin's method is applied to discretize the system. This approach is applicable to simple mechanisms only, because of the difficulty in generating the governing equations for a mechanism with many members; (ii) the mechanism is discretized via a finite element technique, where the nodal displacements are considered as the generalized co-ordinates in the analysis.

The response of the elastic connecting rod in a high-speed slider-crank mechanism was found by Viscomi and Ayre [1] to be dependent upon five parameters: length, mass, damping, external piston force, and frequency. The transient responses in both transverse and longitudinal directions were investigated by Chu and Pan [2].

0022–460X/97/170187 + 15 $25.00/0/sv960832

The Whitworth quick-return mechanism was modified and used for constructing a high-speed impacting press. Dwivedi [3] presented an approximate expression for the angular displacement, velocity and acceleration of the mechanism. The quick-return mechanism was investigated by Beale and Scott [4, 5] focussing on deflection and stability wherein the rod was considered as an Euler–Bernoulli beam. The equation of motion and its boundary conditions were obtained by using Hamilton's principle. Spatial dependence was suppressed by using Galerkin's method with time-dependent pinned–pinned overhanging beam modes. In their following study [6], a large crank case was considered. However, Galerkin's approach was too computationally intensive due to the time-dependent boundary and its complex mode shape.

The finite element discretization approach can be applied to any mechanism. For example, Bahgat and Willmert [7], Song and Haug [8] and Yang and Sadler [9] employed the technique in their work on the dynamics of flexible planar mechanisms. To the authors' knowledge, there is no paper which studies the flexible rod of a quick-return mechanism by the special finite element method with time-dependent shape functions. Generally, by using the Euler beam theory to describe the motion of a flexible rod, the previous studies have neglected the rotary inertia and the shear deformation. In this paper, the Timoshenko and Euler beam theories are used to simulate the flexible rod of a quick-return mechanism as shown in Figure 1. The rod is divided into two regions and each region has a time-dependent length. Hamilton's principle and the finite element method are employed to formulate the governing equation of the flexible rod. Here, it is obvious that the application of the principle is not straightforward, since there is a time-dependent boundary involved. The results of transient amplitude, steady-state response and stable–unstable region are obtained and compared.

2. FORMULATION OF EQUATION OF MOTION

2.1. SYSTEM DESCRIPTION

The quick-return mechanism consists of a crank driving a flexible rod by means of a translating/rotating joint. As shown in Figure 1, $\mathbf{e}_i$ and $\mathbf{e}_j$ are the unit vectors of the rotating

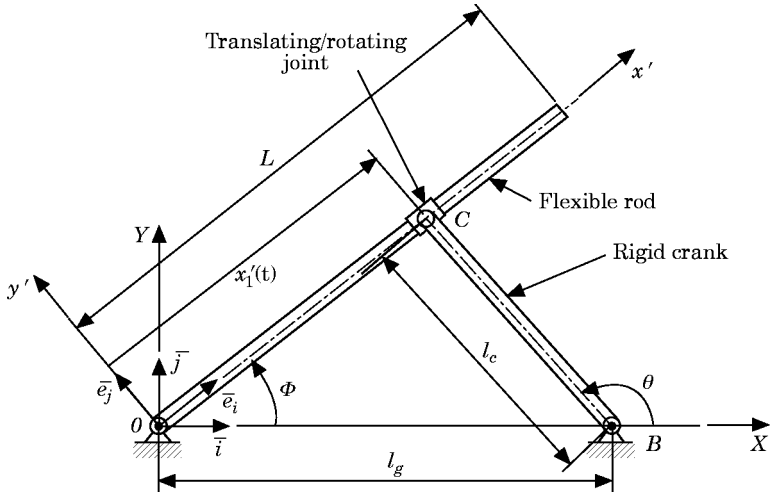

Figure 1. Quick-return mechanism before deformation.

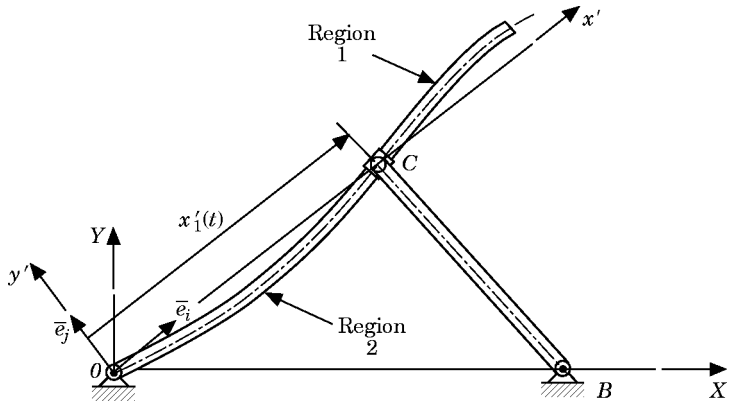

Figure 2. Quick-return mechanism with a flexible rod.

frame $Ox'y'$ which rotates with an angular velocity Φ_t. **i** and **j** are the unit vectors of the fixed frame OXY. $x_1'(t)$ is the current position of the translating/rotating joint. For other symbols in this figure see the nomenclature in Appendix B.

The following assumptions are made in the derivation of the equation of motion: (1) The crank is assumed to be rigid and rotates at a constant angular velocity. (2) The rod is taken to be flexible and is modelled by the Timoshenko and Euler beam theories. (3) The values A, E, I and ρ are taken as constants. (4) The translating/rotating joint is treated as a "knife edge" which is the same as in Beale and Scott [4, 5]. (5) The friction of this joint is neglected.

Because the translating/rotating joint moves reciprocally along the rod, there is a time-dependent boundary involved. The total length L of the flexible rod is divided into two regions as shown in Figure 2. For the finite element analysis, the rod is divided into N_e elements. Region 1 has m elements while region 2 has n elements. Thus, one has $N_e = m + n$. $l_1(t)$ is the element length in region 1 for $x_1'(t) \leqslant x' \leqslant L$ while $l_2(t)$ is the element length in region 2 for $0 \leqslant x' \leqslant x_1'(t)$. The element lengths of the two regions are respectively

$$l_1(t) = (L - x_1'(t))/m, \qquad x_1'(t) \leqslant x' \leqslant L, \qquad l_2(t) = x_1'(\mathrm{t})/n, \qquad 0 \leqslant x' \leqslant x_1'(t), \qquad (1\mathrm{a, b})$$

which satisfy the relationship

$$ml_1(t) + nl_2(t) = L. \qquad (2)$$

2.2. FINITE ELEMENT FORMULATION

The displacement field of the deformed Timoshenko beam is

$$u_1(x, y, t) = u(x, t) - y\psi(x, t), \qquad u_2(x, y, t) = v(x, t), \qquad (3)$$

where u and v represent the axial and transverse displacements of the flexible rod respectively, and ψ is the slope of the deflection curve due to bending deformation alone.

In order to assemble the elements and to equate the corresponding co-ordinates, a transformation of element variable is necessary. In this paper, the rotating co-ordinate system $Ox'y'$ fixed on the flexible rod is selected to be the reference co-ordinate. Figure 3 shows the ith beam element undergoing gross motion and elastic deformation. The deformed position vector of an arbitrary point P in the ith element is

$$\mathbf{R}(x, y, t) = R^i(t)\mathbf{e}_\mathbf{i} + (x + u_1)\mathbf{e}_\mathbf{i} + u_2\mathbf{e}_\mathbf{j}, \qquad (4)$$

where vector $R^i(t)\mathbf{e_i}$ locates the origin o' of the local co-ordinate system $o'xy$ of the ith beam element. Thus, the length $R^i(t)$ in regions 1 and 2 are respectively

$$R^i(t) = \begin{cases} nl_2(t) + (i-1)l_1(t), & i = 1, 2, \ldots, m; \\ (i-1)l_2(t), & i = 1, 2, \ldots, n. \end{cases} \tag{5}$$

By differentiating equation (4) with respect to time t, the absolute velocity vector is

$$\mathbf{R_t}(x, y, t) = [R_t^i + u_t - y\psi_t - v\Phi_t]\mathbf{e_i} + [(R^i + x + u - y\psi)\Phi_t + v_t]\mathbf{e_j}. \tag{6}$$

The kinetic energy for the ith element is given by

$$T_i = \frac{1}{2}\int_{V_e} \rho \mathbf{R_t} \cdot \mathbf{R_t}\, \mathrm{d}V_e$$

$$= \frac{1}{2}\int_0^{l(t)} \rho A\{[R_t^i + u_t - v\Phi_t]^2 + [(R^i + x + u)\Phi_t + v_t]^2\} + \rho I[\psi_t^2 + \Phi_t^2\psi^2]\, \mathrm{d}x, \tag{7}$$

where $l(t)$ is used to represent the element length $l_1(t)$ in region 1 and the element length $l_2(t)$ in region 2.

The Lagrange linear strains are

$$\epsilon_{xx} = u_x - y\psi_x, \qquad \epsilon_{yy} = 0, \qquad \epsilon_{xy} = \tfrac{1}{2}(v_x - \psi), \tag{8}$$

where the high order terms $\frac{1}{2}\psi^2$, $u_x\psi$ and $y\psi\psi_x$ are neglected. The strain energy for the ith element due to bending, axial and shear deformations is

$$U_i = \frac{1}{2}\int_{V_e} \sigma_{ij}\epsilon_{ij}\, \mathrm{d}V_e = \frac{1}{2}\int_0^{l(t)} \{EAu_x^2 + EI\psi_x^2 + KGA(v_x - \psi)^2\}\, \mathrm{d}x. \tag{9}$$

The kinetic energy of crank with mass M_c and mass momentum of inertia J_c is

$$T_{crank} = \tfrac{1}{8}M_c l_c^2\dot{\theta}^2 + \tfrac{1}{2}J_c\dot{\theta}^2. \tag{10}$$

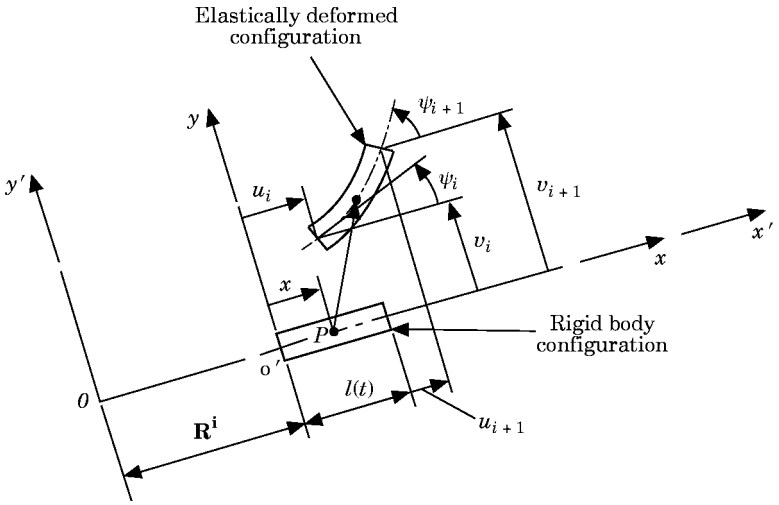

Figure 3. The ith beam element undergoing gross motion and elastic deformation.

Note that the variation of the crank kinetic energy is zero since $\dot{\theta}$ is prescribed. The Lagrangian function is the kinetic energy minus the potential energy. Hence, it is a function of the unknown deformations u, v and ψ which are functions of position x and time t. It is seen from the kinetic energy (7) and the strain energy (9) that the effect of the time-dependent length is included in the Lagrangian function.

The usual approach in the finite element method is to assume each unknown deformation $w(x, t)$ to be approximated by a finite series in the following form

$$w(x, t) = \sum_{i=1}^{N_e+1} N_i(x, l(t))q_i(t), \tag{11}$$

where $N_e + 1$ is the total number of nodal points, $q_i(t)$ represents the nodal displacement, and $N_i(x, l(t))$ is a function of x and $l(t)$. The finite series (11) permits the evaluations of the integrals in equations (7) and (9), and the Lagrangian becomes a function of the unknown nodal displacement $q_i(t)$.

To provide continuity at the intersections of the finite elements, three nodal deflections at each end of an element will be introduced. The displacements at each nodal point is assumed to be composed of the axial deformation u, transverse deformation v and rotation ψ. The choice of the function $N_i(x, l(t))$ has a significant effect on the accuracy of the solution and the size of the problem [9].

In this paper, the Hermite polynomials are selected to represent the functions $N_i(x, l(t))$ which is the same as in Bahgat and Willmert [7]. The unknown deformations u, v and ψ are approximated as follows

$$\begin{Bmatrix} u \\ v \\ \psi \end{Bmatrix} = \begin{bmatrix} N_{u_1} & 0 & 0 & N_{u_2} & 0 & 0 \\ 0 & N_{v_1} & N_{v_2} & 0 & N_{v_3} & N_{v_4} \\ 0 & N_{\psi_1} & N_{\psi_2} & 0 & N_{\psi_3} & N_{\psi_4} \end{bmatrix} \{\mathbf{q}\}_i, \tag{12}$$

where $\{\mathbf{q}\}_i = [u_i, v_i, \psi_i, u_{i+1}, v_{i+1}, \psi_{i+1}]^T$ is the nodal displacement vector for the ith element, and $N_{u1}, N_{u2}, \ldots, N_{v3}, N_{v4}, \ldots, N_{\psi3}, N_{\psi4}$ are the general Hermite polynomials. Details of the shape functions are given in Appendix A. It should be noted that these shape functions are time-dependent.

The derivatives of u and v, the curvature κ and the shear strain γ within the ith element can be written as

$$u_x = \mathrm{d}u/\mathrm{d}x \equiv [B_u]\{\mathbf{q}\}_i, \qquad \kappa = \mathrm{d}\psi/\mathrm{d}x \equiv [B_b]\{\mathbf{q}\}_i, \tag{13a, b}$$

$$v_x = \mathrm{d}v/\mathrm{d}x \equiv [B_v]\{\mathbf{q}\}_i, \qquad \gamma = \mathrm{d}v/\mathrm{d}x - \psi \equiv [B_s]\{\mathbf{q}\}_i, \tag{13c, d}$$

where

$$[B_u] = \frac{\mathrm{d}}{\mathrm{d}x}[N_u], \qquad [B_b] = \frac{\mathrm{d}}{\mathrm{d}x}[N_\psi], \qquad [B_v] = \frac{\mathrm{d}}{\mathrm{d}x}[N_v], \qquad [B_s] = \frac{\mathrm{d}}{\mathrm{d}x}[N_v] - [N_\psi].$$

The shape functions are substituted into the kinetic energy T_i of (7) and the strain energy U_i of (9), and then T_i and U_i can be rewritten in terms of the nodal displacement $\{\mathbf{q}\}_i$ as

$$T_i = \tfrac{1}{2}\{\dot{\mathbf{q}}\}_i^T[\mathbf{m}_1]\{\dot{\mathbf{q}}\}_i + \tfrac{1}{2}\{\mathbf{q}\}_i^T[\mathbf{m}_2]\{\mathbf{q}\}_i + \{\mathbf{q}\}_i^T[\mathbf{m}_c]\{\dot{\mathbf{q}}\}_i + [\mathbf{m}_{qt}]\{\dot{\mathbf{q}}\}_i + [\mathbf{m}_q]\{\mathbf{q}\}_i + Z^* \tag{14}$$

$$U_i = \tfrac{1}{2}\{\mathbf{q}\}_i^T([\mathbf{K}_u] + [\mathbf{K}_s] + [\mathbf{K}_b])\{\mathbf{q}\}_i \tag{15}$$

where the matrices $[\mathbf{m}_1]$, $[\mathbf{m}_2]$, $[\mathbf{m}_c]$, $[\mathbf{m}_{qt}]$, $[\mathbf{m}_q]$, $[\mathbf{K}_u]$, $[\mathbf{K}_s]$, $[\mathbf{K}_b]$ and Z^* are all functions of $l(t)$. For the details see Appendix A.

2.3. HAMILTON'S PRINCIPLE

Since there is a moving boundary involved, the element length, mass and stiffness matrices are time-dependent. Hamilton's principle is

$$0 = \delta \int_{t_1}^{t_2} \sum_{i=1}^{N_e} L_i \, \mathrm{d}t \tag{16}$$

where N_e is the total number of elements of the flexible rod and the Lagrangian function of each element is $L_i = T_i - U_i$. Performing the variation on the Lagrangian function of each element, one obtains

$$0 = \int_{t_1}^{t_2} \left[\sum_{i=1}^{m} \delta\{\mathbf{q}\}_i^{\mathrm{T}} \left(\frac{\partial L_i}{\partial \{\mathbf{q}\}_i} - \frac{\mathrm{d}}{\mathrm{d}t} \frac{\partial L_i}{\partial \{\dot{\mathbf{q}}\}_i} \right) + \sum_{j=1}^{n} \delta\{\mathbf{q}\}_j^{\mathrm{T}} \left(\frac{\partial L_j}{\partial \{\mathbf{q}\}_j} - \frac{\mathrm{d}}{\mathrm{d}t} \frac{\partial L_j}{\partial \{\dot{\mathbf{q}}\}_j} \right) \right] \mathrm{d}t$$

$$+ \left[\sum_{i=1}^{m} \delta\{\mathbf{q}\}_i^{\mathrm{T}} \frac{\partial L_i}{\partial \{\dot{\mathbf{q}}\}_i} + \sum_{j=1}^{n} \delta\{\mathbf{q}\}_j^{\mathrm{T}} \frac{\partial L_j}{\partial \{\dot{\mathbf{q}}\}_j} \right]_{t_1}^{t_2}, \tag{17}$$

where m and n are the element numbers of regions 1 and 2, respectively. The varied path coincides with the true path at the two timing ends t_1 and t_2. It follows that $\delta q_i(t_1) = \delta q_i(t_2) = 0$ and $\delta q_j(t_1) = \delta q_j(t_2) = 0$. In differentiating with respect to time, it must be remembered that the element length is time-dependent. The element matrices, therefore, are functions of time, and depend on the rigid-body motion of the mechanism as well as the integrals of the products of the Hermite polynomials.

Since the translating/rotating joint is assumed to be a knife edge, the displacement and slope are continuous across the joint. Combining regions 1 and 2, the global ordinary differential equation is obtained as

$$[\mathbf{M}]\{\ddot{\mathbf{Q}}\} + [\mathbf{C}]\{\dot{\mathbf{Q}}\} + [\mathbf{K}]\{\mathbf{Q}\} = \{\mathbf{F}\} \tag{18}$$

where

$$\{\mathbf{Q}\} = \{u_1, v_1, \psi_1, u_2, v_2, \psi_2, \ldots, u_{N_{e+1}}, v_{N_{e+1}}, \psi_{N_{e+1}}\}^{\mathrm{T}},$$

[**M**] and [**K**] are the global mass and stiffness matrices, respectively, [**C**] is the global damping term, and {**F**} is the force term.

The mass, damping, and stiffness matrices in equation (18) are all functions of the rigid-body motion of the mechanism and therefore the kinematics of the mechanism must be solved first. Once this is obtained, equation (18) can be used to solve the global deflection vector **Q**. The rigid-body motion is of the form

$$\theta = \Omega t + \theta_0, \qquad \dot{\theta} = \Omega, \qquad \Phi = \sin^{-1}\left(\frac{l_c \sin\theta}{(l_g^2 + l_c^2 + 2 l_g l_c \cos\theta)^{1/2}} \right),$$

$$\dot{\Phi} = \frac{l_c \dot{\theta} \cos(\theta - \Phi)}{x_1'}, \tag{19a–d}$$

$$\ddot{\Phi} = \frac{l_g l_c \dot{\theta}^2 (l_c^2 - l_g^2) \sin\theta}{x_1'^4}, \qquad x_1' = (l_g^2 + l_c^2 + 2 l_g l_c \cos\theta)^{1/2}, \qquad \dot{x}_1' = \frac{-l_g l_c \dot{\theta} \sin\theta}{x_1'}. \tag{19e–g}$$

If the slenderness ratio is very small, the shear deformation can be neglected compared

to the flexural deformations. Euler beam theory can be used to describe the motion of the flexible rod by setting

$$\psi = v_x \tag{20}$$

and neglecting the rotary inertia term $\rho I[(\Phi_t + \psi_t)^2 + \Phi_t^2\psi^2]$. For the Euler beam theory, the value ϕ in Appendix A is set equal to zero, that is, take $KG \to \infty$ [10].

The quick-return mechanism in this paper is divided into a large crank problem and a small crank one. The transient amplitudes of the large crank problem, for example, the Whitworth crank shaper, are obtained by using the Runge–Kutta numerical method to integrate equation (18). The steady state responses and the dynamic stability analysis of the small crank problem, for example, the sewing machine, are to be analyzed in the following sections.

3. DYNAMIC STABILITY ANALYSIS

Since the frequency of the axial deformation is much larger than that of the practical operation, the axial deformation is neglected in the dynamic stability analysis and the equations of transverse deformation become uncoupled. Thus, only the dynamic stability analysis of the transverse deformation is investigated in this paper. With the small crank case, the non-dimensional parameter ϵ is defined as

$$\epsilon = l_c/l_g \tag{21}$$

where l_g is the length of ground link, and l_c is the crank length. For a small crank ($\epsilon \ll 1$), all coefficient matrices of equation (18) can be simplified by applying the binomial expansion. Now, x_1', $\dot{x}_1'$, $\dot{\Phi}$ and $\ddot{\Phi}$ become functions of θ and ϵ:

$$x_1' = l_g(1 + \epsilon\cos\theta) + \text{H.O.T.}, \qquad x_1' = -l_g\epsilon\dot{\theta}\sin\theta + \text{H.O.T.}, \tag{22a, b}$$

$$\dot{\Phi} = \epsilon\dot{\theta}\cos\theta + \text{H.O.T.}, \qquad \ddot{\Phi} = -\epsilon\dot{\theta}^2\sin\theta + \text{H.O.T.}. \tag{22c, d}$$

Substituting the above equations (22a–d) into the element matrices in Appendix A, retaining the terms up to $\mathcal{O}(\epsilon)$, and assembling all element equations, one obtains the global equation for the small crank problem as

$$([\mathbf{M}_A] + \epsilon[\mathbf{M}_B]\cos\theta)\{\ddot{\mathbf{Q}}\} + \epsilon\mathbf{\Omega}[\mathbf{C}_A]\sin\theta\{\dot{\mathbf{Q}}\} + ([\mathbf{K}_A] + \epsilon[\mathbf{K}_B]\cos\theta)\{\mathbf{Q}\} = \epsilon[\mathbf{F}_A]\sin\theta. \tag{23}$$

The detailed expressions of $[\mathbf{M}_A]$, $[\mathbf{M}_B]$, $[\mathbf{C}_A]$, $[\mathbf{K}_A]$, $[\mathbf{K}_B]$ and $[\mathbf{F}_A]$ are given in Lee [11], and they are all constant matrices. Equation (23) represents a system of the second-order differential equations with periodic coefficients of the Mathieu–Hill type.

Beale and Scott [4–6] showed that the instability could also arise due to the inhomogeneous solution. Nevertheless, the parametric stability of the homogeneous solution of equation (23) will be investigated in this paper. According to the theory of linear equations with periodic coefficients [12], the boundaries between stable and unstable regions can be constructed by the periodic solutions with period T and $2T$ where $T = 2\pi/\Omega$.

It was demonstrated [12] that the solutions with period $2T$ are of the greatest practical importance for parametric resonance. With a view toward constructing a solution of the homogeneous part of the system (23) with period $2T$, one sets

$$\mathrm{Q}(t) = \sum_{k=1,3,5\cdots}^{\infty} \left(\{a_k\}\sin\frac{k\Omega t}{2} + \{b_k\}\cos\frac{k\Omega t}{2} \right). \tag{24}$$

By substituting equation (24) into the homogeneous part of equation (23) and equating the coefficient of the sin $k\Omega t/2$ and cos $k\Omega t/2$ terms, a set of linear homogeneous algebraic equations in terms of $\{a_k\}$ and $\{b_k\}$ is obtained as

$$\{[\mathbf{K}_A] - \tfrac{1}{2}\epsilon[\mathbf{K}_B] - [\Omega^2/4]([\mathbf{M}_A] - [\epsilon/2]([\mathbf{M}_B] + [\mathbf{C}_A]))\} \cdot \{a_1\} + [\epsilon/2]([\mathbf{K}_B] - [3\Omega/2][\mathbf{C}_A] - [9\Omega^2/4][\mathbf{M}_B])\{a_3\} = 0, \tag{25a}$$

$$\tfrac{1}{2}\epsilon\{-[(r+2)^2\Omega^2/4][\mathbf{M}_B] - [(r+2)\Omega^2/2][\mathbf{C}_A] + [\mathbf{K}_B]\}\{a_{r+2}\} \cdot \{-[r^2\Omega^2/4][\mathbf{M}_A] + [\mathbf{K}_A]\}\{a_r\} + \tfrac{1}{2}\epsilon\{-[(r-2)^2\Omega^2/4][\mathbf{M}_B] - [(r-2)^2\Omega^2/2][\mathbf{C}_A] + [\mathbf{K}_B]\}\{a_{r-2}\} = \{0\}, \quad (r = 3, 5, 7, \ldots), \tag{25b}$$

$$\{[\mathbf{K}_A] - \tfrac{1}{2}\epsilon[\mathbf{K}_B] - [\Omega^2/4]([\mathbf{M}_A] + [\epsilon/2]([\mathbf{M}_B] + [\mathbf{C}_A]))\}\{b_1\} + [\epsilon/2]([\mathbf{K}_B] - [3\Omega/2][\mathbf{C}_A] - [9\Omega^2/4][\mathbf{M}_B])\{b_3\} = 0, \tag{25c}$$

$$\tfrac{1}{2}\epsilon\{-[(r+2)^2\Omega^2/4][\mathbf{M}_B] - [(r+2)\Omega^2/2][\mathbf{C}_A] + [\mathbf{K}_B]\}\{b_{r+2}\} + \{-[r^2\Omega^2/4][\mathbf{M}_A] + [\mathbf{K}_A]\}\{b_r\} + \tfrac{1}{2}\epsilon\{-[(r-2)^2\Omega^2/4][\mathbf{M}_B] + [(r-2)\Omega^2/2][\mathbf{C}_A] + [\mathbf{K}_B]\}\{b_{r-2}\} = \{0\}, \quad (r = 3, 5, 7, \ldots). \tag{25d}$$

The condition for the set of linear homogenous equations (25a–d) to have a non-trivial solution is used to calculate the boundaries of the stable–unstable region [12]. However, the method used in this paper fails to capture the combination type instability. The stable–unstable zones of the combination resonance were determined by Beale and Scott [4, 5] where Hsu's method was employed.

4. STEADY-STATE ANALYSIS OF TIME-VARYING SYSTEM

The steady-state responses of the equation (23) with harmonic excitation can be determined by the harmonic balance method. The periodic solutions with period T can be expressed in Fourier series as

$$\mathrm{Q}(t) = \tfrac{1}{2}\{b_0\} + \sum_{k=2,4,6\cdots}^{\infty}\left(\{a_k\}\sin\frac{k\Omega t}{2} + \{b_k\}\cos\frac{k\Omega t}{2}\right). \tag{26}$$

Substituting equation (26) into equation (23) and collecting the coefficients in the same harmonic term, one can obtain a system of the non-homogeneous algebraic equations in terms of $\{a_k\}$ and $\{b_k\}$ as

$$([\mathbf{K}_A] - \Omega^2[\mathbf{M}_A])\{\mathbf{a}_2\} + \epsilon(\tfrac{1}{2}[\mathbf{K}_B] - \Omega^2[\mathbf{C}_A] - 2\Omega^2[\mathbf{M}_B])\{a_4\} = [\mathbf{F}_A], \tag{27a}$$

$$\tfrac{1}{2}\epsilon\{-[(r+2)^2\Omega^2/4][\mathbf{M}_B] - [(r+2)\Omega^2/2][\mathbf{C}_A] + [\mathbf{K}_B]\}\{a_{r+2}\} \cdot \{-[r^2\Omega^2/4][\mathbf{M}_A] + [\mathbf{K}_A]\}\{a_r\} + \tfrac{1}{2}\epsilon\{-[(r-2)^2\Omega^2/4][\mathbf{M}_B] - [(r-2)^2\Omega^2/2][\mathbf{C}_A] + [\mathbf{K}_B]\}\{a_{r-2}\} = \{0\}, \quad (r = 4, 6, 8, \ldots), \tag{27b}$$

$$\tfrac{1}{2}[\mathbf{K}_A]\{b_0\} - \tfrac{1}{2}(\Omega^2[\mathbf{M}_B] - \Omega^2[\mathbf{C}_A] + [\mathbf{K}_B])\{b_2\} = \{0\}, \tag{27c}$$

$$\tfrac{1}{2}\epsilon[\mathbf{K}_B]\{b_0\} + ([\mathbf{K}_A] - \Omega^2[\mathbf{M}_B])\{b_2\} + \epsilon(\tfrac{1}{2}[\mathbf{K}_B] - \Omega^2[\mathbf{C}_A] - 2\Omega^2[\mathbf{M}_B])\{b_4\} = \{0\}, \tag{27d}$$

$$\tfrac{1}{2}\epsilon\{-[(r+2)^2\Omega^2/4][\mathbf{M}_B] - [(r+2)\Omega^2/2][\mathbf{C}_C] + [\mathbf{K}_B]\}\{b_{r+2}\} + \{-[r^2\Omega^2/4][\mathbf{M}_A] + [\mathbf{K}_A]\}\{b_r\} + \tfrac{1}{2}\epsilon\{-[(r-2)^2\Omega^2/4][\mathbf{m}_2] + [(r-2)\Omega^2/2][\mathbf{C}_A] + [\mathbf{K}_B]\}\{b_{r-2}\} = \{0\}, \quad (r = 4, 6, 8, \ldots). \tag{27e}$$

TABLE 1

Comparison of the natural frequencies (rad/s).

Mode	Exact	Present work			Beale [4]
		Two elements	Four elements	Six elements	
First	858·3	861·1	858·4	858·3	904·1
Second	2630·0	3136·5	2646·7	2633·6	3369·0
Third	7255·7	8886·9	7606·5	7395·5	10714·5

The total amplitude of the periodic solution can be written as

$$A_p = \sum_{k=2,4,6\cdots}^{r} (\{a_k\}^2 + \{b_k\}^2)^{1/2}, \tag{28}$$

where r is chosen large enough such that $\{a_r\}$ and $\{b_r\}$ are sufficiently small and negligible.

5. NUMERICAL RESULTS AND DISCUSSIONS

In the large crank problem, the example of a rod has the same material properties and dimensions as in Beale [4] and Bahagat and Willmert [6]. The example involves the following dimensions and properties: $l_c = 1{\cdot}5$ in, $l_g = 4{\cdot}0$ in, $L = 9{\cdot}3746$ in, $\rho = 0{\cdot}000725$ lb in^{-4} s^2, $EI = 2{\cdot}91992$E6 lbf in^2, $A = 0{\cdot}4531$ in^2, $K = 0{\cdot}9$, $G = 11\,800$ lb/in^2, $\dot{\theta} = 90$ rad/s, $\theta(0) = -135^\circ$.

This example differs from the small crank in that not only is the rod stiffer, but the greater stiffness also increases the computation time required to run for 1 cycle of crank motion. Now, the flexible rod is divided into two, four and six elements, and the natural frequencies are found and compared with those of Beale [4] approximated by the polynomial modes. The results are shown in Table 1, where the exact natural frequencies of the first three modes are the pinned–pinned overhanging beam when the crank does not rotate. It can be seen that when four elements are taken in the analysis, good accuracy is obtained.

Using the Runge–Kutta numerical method, one can obtain the transient amplitudes of the flexible rod modelled by the Timoshenko and Euler beam theories. Figure 4 shows the computed results with a small amount of the damping being introduced into the equation. Here the damping term is taken to be 0·002 times the sum of the mass and stiffness matrices. It is observed that the damping term absorbs the amplitudes of the high frequency modes.

Owing to the rotary inertia and the shear deformation being taken into account, the transient deflections obtained by Timoshenko beam theory are larger than those simulated by the Euler beam theory (Figures 5–7). In these figures, the computation time is 2 cycles of crank motion.

The other example of the flexible rod has the following dimensions and properties: $L = 1$ m, $l_g = 0{\cdot}5997$ m, $E = 0{\cdot}7$E11 N/m^2, $A = 0{\cdot}0025$ m^2, $I = 0{\cdot}5208\text{E} - 6$ m^4, $\bar{m} = 7{\cdot}15$ kg/m, $K = 0{\cdot}85$, $G = 0{\cdot}269$E11 N/m^2, which are the same as the sewing machine studied by Gurgöze [13]. For the dynamic stability analysis, the stable–unstable regions of the flexible rod are shown in Figures 8 and 9. The instability zones emanate from the frequency ratio axis at points where $\epsilon = 0$. Figure 8 shows the instability zones for modes 1 and 2, in which the flexible rod is simulated by Euler beam theory and is divided into

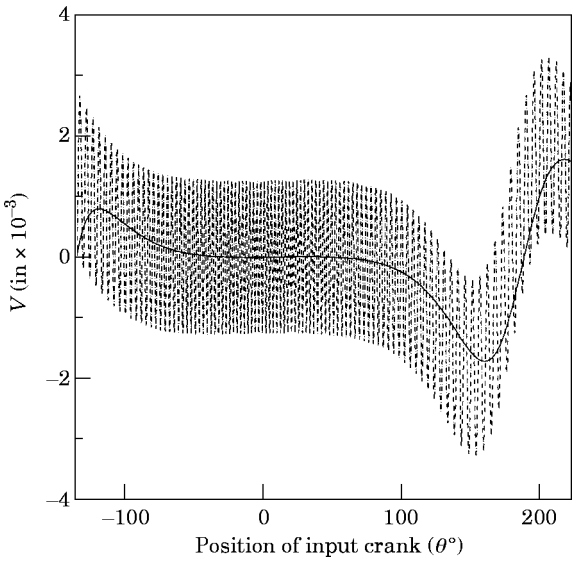

Figure 4. Euler beam tip transverse deflection: - - -, without damping; ——, 0·002 damping.

two, four, and six elements. It is seen that as the number of elements increases, the unstable region shifts toward the direction of the lower frequency ratio. Figure 9 compares the stable–unstable regions between the Timoshenko and the Euler beams for the first four modes. In this figure, four elements are taken in the finite element method. As the shear deformation and the rotary inertia are considered, the regions of dynamic instability are shifted closer to each other and the widths of these regions are increased. It is seen that the regions in the higher modes are greatly affected.

The effect of the non-dimensional crank ratio ϵ on the steady state response is shown in Figure 10 where ϵ is taken as 0·02, 0·05 and 0·08. Figures 10(a) and (b) show the

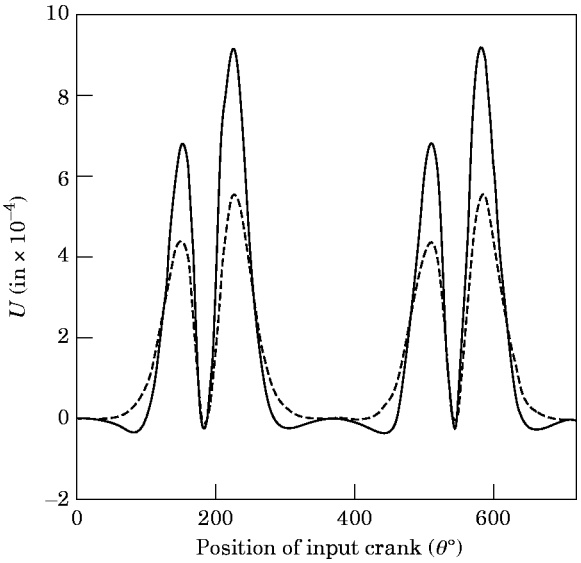

Figure 5. The axial displacement at tip end: - - -, Euler beam; ——, Timoshenko beam.

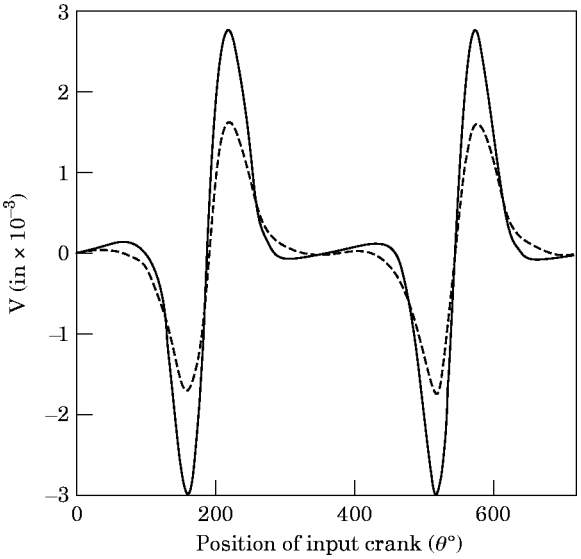

Figure 6. The transverse displacement at tip end: - - -, Euler beam; ——, Timoshenko beam.

steady-state responses of the Euler beam with linear and logarithmic scales respectively. From the results shown in Fig. 10(b), it is revealed that the amplification of the non-homogeneous solution is at speeds ω_n/N where N is an integer, and the increase in ϵ is related to the increase in the amplification of the steady-state responses.

6. CONCLUSION

The flexible rod of a high-speed quick-return mechanism has been modelled by the Timoshenko and Euler beam theories. The finite element method and Hamilton's principle were employed to derive the governing equations. Since the element length is

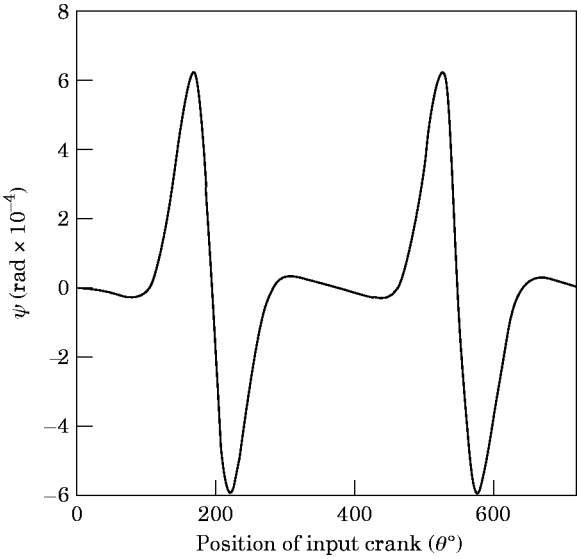

Figure 7. The rotation displacement at the Timoshenko-beam tip.

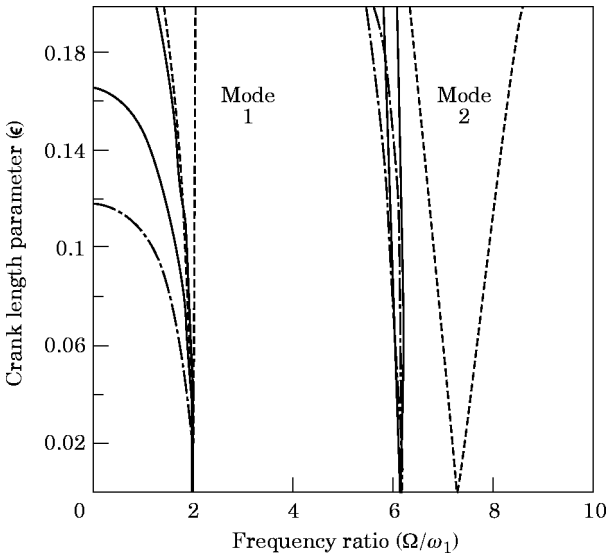

Figure 8. Euler beam instability zones for modes 1 and 2: - - -, 2 elements; ——, 4 elements; –·–·, 6 elements.

time-dependent, the governing equation has time-varying coefficients. In the large crank problem, the transient amplitudes were obtained and compared between the Timoshenko and Euler beam theories. In the small crank problem, the steady state response and dynamic stability of the flexible rod are analyzed. From the results of transient amplitude, steady-state response and dynamic stability, the following conclusions are drawn:

(1) The transient amplitudes of the flexible rod modelled by the Timoshenko beam theory are larger than those modelled by the Euler beam theory. For the small crank case, all the results are periodic.

(2) As the number of elements increases in the analysis, the unstable region shifts towards the direction of the lower frequency ratio. Due to the shear deformation and the

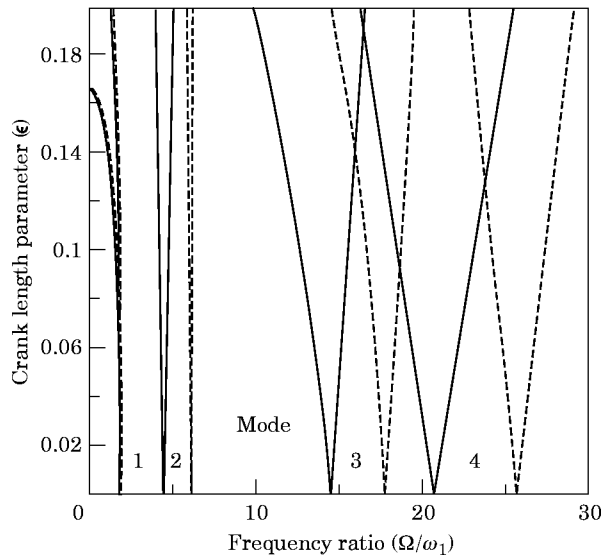

Figure 9. Instability zones for the first 4 modes with 4 elements: - - -, Euler beam; ——, Timoshenko beam.

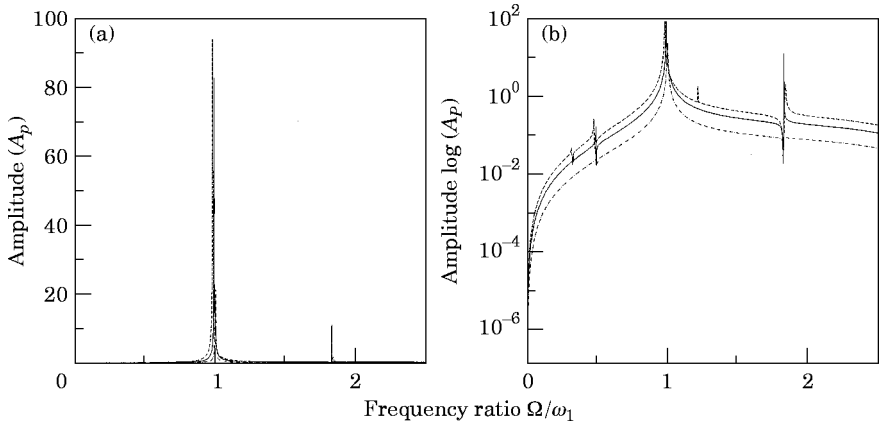

Figure 10. Euler beam steady-state response: (a) Ω/ω_1 versus A_p; (b) Ω/ω_1 versus log (A_p). $\epsilon =$: —·—·, 0·02; ——,0·05; - - -, 0·08.

rotary inertia being considered, the regions of dynamic instability are broadened and are shifted closer to each other.

(3) As the crank length ratio increases, the steady-state response and the amplification of the non-homogeneous solution increase.

ACKNOWLEDGMENT

Support of this work by the National Science Council of the Republic of China under Contract NSC 84-2212-E-033-009 is gratefully acknowledged.

REFERENCES

1. B. V. Viscomi and B. S. Ayre 1979 *American Society of Mechanical Engineers Journal of Engineering for Industry* **101,** 251–262. Nonlinear dynamic response of elastic slider-crank mechanism.
2. S. C. Chu and K. C. Pan 1975 *American Society of Mechanical Engineers Journal of Engineering for Industry* **97,** 542–550. Dynamic response of a high speed slider-crank with an elastic connecting rod.
3. S. N. Dwivedi 1984 *Mechanism and Machine Theory* **19,** 51–59. Application of Whitworth quick return mechanism for high velocity impacting press.
4. D. G. Beale 1988 *Phd Dissertation*, *University of Michigan*. A study of the motion of a flexible rod in a quick return mechanism.
5. D. G. Beale and R. A. Scott 1990 *Journal of Sound and Vibration* **141,** 277–289. The stability and response of a flexible rod in a quick return mechanism.
6. D. G. Beale and R. A. Scott 1993 *Journal of Sound and Vibration* **166,** 277–289. The stability and response of a flexible rod in a quick return mechanism: large crank case.
7. B. M. Bahgat and K. D. Willmert 1976 *Mechanism and Machine Theory* **11,** 47–71. Finite element vibrational analysis of planar mechanisms.
8. J. O. Song and E. J. Haug 1980 *Computer Methods in Applied Mechanics and Engineering* **24,** 359–381. Dynamic analysis of planar flexible mechanisms.
9. Z. Yang and J. P. Sadler 1990 *American Society of Mechanical Engineers Journal of Mechanical Design* **112,** 175–182. Large-displacement finite element analysis of flexible linkages.
10. H. Reismann and P. S. Pawlik 1980 *Elasticity Theory and Application*. London: John Wiley, chapter 6.
11. F. Y. Lee 1993 *Master Thesis*, *Chung-Yuan Christian University*, *Chung-Li*, *Taiwan*. Dynamic stability of a high-speed quick-return mechanism with a flexible rod.

12. V. V. BOLOTIN 1964 *The Dynamic Stability of Elastic Systems*. San Francisco: Holden-Day Inc.
13. M. GURGÖZE 1985 *Zeitschrift für angewandte Mathematik und Mechanik* **65,** 451–454. Ein beitrag zum stabilitatsverhalten einer pendelnden kurb elschleife.

APPENDIX A

Shape functions of equation (12) are

$$N_{u_1} = 1 - \frac{x}{l(t)}, \qquad N_{u_2} = \frac{x}{l(t)}, \qquad N_{v_1} = \frac{[l(t)^3 - 3x^2 l(t) + 2x^3 + (l(t)^3 - xl(t)^2)\phi]}{l(t)^3(1+\phi)},$$

$$N_{v_2} = \frac{[(xl(t)^2 - 2x^2 l(t) + x^3 + (xl(t)^2 - x^2 l(t))\phi/2]}{l(t)^2(1+\phi)}, \qquad N_{v_3} = \frac{(3x^2 l(t) - 2x^3 + xl(t)^2\phi)}{l(t)^3(1+\phi)},$$

$$N_{v_4} = \frac{[-x^2 l(t) + x^3 - (xl(t)^2 - x^2 l(t))\phi/2]}{l(t)^2(1+\phi)}, \qquad N_{\psi_1} = \frac{6(-xl(t) + x^2)}{[l(t)^3(1+\phi)]},$$

$$N_{\psi_2} = \frac{[l(t)^2 - 4xl(t) + 3x^2 + (l(t)^2 - xl(t))\phi]}{l(t^2)(1+\phi)}, \qquad N_{\psi_3} = \frac{6(xl(t) - x^2)}{[l(t)^3(1+\phi)]},$$

$$N_{\psi_4} = \frac{(-2xl(t) + 3x^2 + xl(t)\phi)}{l(t)^2(1+\phi)}, \qquad \phi = \frac{12EI}{KGAl(t)^2}$$

Coefficient matrices of equations (14) and (15) are

$$[\mathbf{m}_1] = \rho A \int_0^{l(t)} \{[\mathbf{N}_u]^{\mathrm{T}}[\mathbf{N}_u] + [\mathbf{N}_v]^{\mathrm{T}}[\mathbf{N}_v]\}\,\mathrm{d}x + \rho I \int_0^{l(t)} [\mathbf{N}_\psi]^{\mathrm{T}}[\mathbf{N}_\psi]\,\mathrm{d}x$$

$$[\mathbf{m}_2] = \rho A \int_0^{l(t)} \{[\dot{\mathbf{N}}_u]^{\mathrm{T}}[\dot{\mathbf{N}}_u] + [\dot{\mathbf{N}}_v]^{\mathrm{T}}[\dot{\mathbf{N}}_v]\}\,\mathrm{d}x + \rho A \Phi_t \int_0^{l(t)} \{[\mathbf{N}_u]^{\mathrm{T}}[\dot{\mathbf{N}}_v] + [\dot{\mathbf{N}}_v]^{\mathrm{T}}[\mathbf{N}_u]$$

$$- [\dot{\mathbf{N}}_u]^{\mathrm{T}}[\mathbf{N}_v] - [\mathbf{N}_v]^{\mathrm{T}}[\dot{\mathbf{N}}_u]\}\,\mathrm{d}x + \rho A \Phi_t^2 \int_0^{l(t)} \{[\mathbf{N}_u]^{\mathrm{T}}[\mathbf{N}_u] + [\mathbf{N}_v]^{\mathrm{T}}[\mathbf{N}_v]\}\,\mathrm{d}x$$

$$+ \rho I \Phi_t^2 \int_0^{l(t)} [\mathbf{N}_\psi]^{\mathrm{T}}[\mathbf{N}_\psi]\,\mathrm{d}x + \int_0^{l(t)} [\dot{\mathbf{N}}_\psi]^{\mathrm{T}}[\dot{\mathbf{N}}_\psi]\,\mathrm{d}x$$

$$[\mathbf{m}_c] = \rho A \left(\Phi_t \int_0^{l(t)} \{[\mathbf{N}_u]^{\mathrm{T}}[\mathbf{N}_v] - [\mathbf{N}_v]^{\mathrm{T}}[\mathbf{N}_u]\}\,\mathrm{d}x + \int_0^{l(t)} \{[\dot{\mathbf{N}}_u]^{\mathrm{T}}[\mathbf{N}_u] + [\dot{\mathbf{N}}_v]^{\mathrm{T}}[\mathbf{N}_v]\}\,\mathrm{d}x \right)$$

$$+ \rho I \int_0^{l(t)} [\dot{\mathbf{N}}_\psi]^{\mathrm{T}}[\mathbf{N}_\psi]\,\mathrm{d}x$$

$$[\mathbf{m}_{qt}] = \rho A \int_0^{l(t)} \{\Phi_t(\mathbf{R}^i + x)[\mathbf{N}_v]^{\mathrm{T}} + \mathbf{R}_t^i[\mathbf{N}_u]^{\mathrm{T}}\}\,\mathrm{d}x$$

$$[\mathbf{m}_q] = \rho A \int_0^{l(t)} \{\Phi_t(\mathbf{R}^i + x)(\Phi_t[\mathbf{N}_u]^{\mathrm{T}} + [\dot{\mathbf{N}}_v]^{\mathrm{T}}) + \mathbf{R}_t^i([\dot{\mathbf{N}}_u]^{\mathrm{T}} - \Phi_t[\mathbf{N}_v]^{\mathrm{T}})\}\,\mathrm{d}x$$

$$Z^* = \tfrac{1}{2}\rho A \int_0^{l(t)} [\Phi_i^2(\mathbf{R}^i + x)^2 + (\mathbf{R}_t^i)^2]\,\mathrm{d}x$$

$$[\mathbf{K}_u] = EA \int_0^{l(t)} [\mathbf{B}_u]^{\mathrm{T}}[\mathbf{B}_u]\,\mathrm{d}x, \qquad [\mathbf{K}_b] = EI \int_0^{l(t)} [\mathbf{B}_b]^{\mathrm{T}}[\mathbf{B}_b]\,\mathrm{d}x$$

$$[\mathbf{K}_s] = KGA \int_0^{l(t)} [\mathbf{B}_s]^{\mathrm{T}}[\mathbf{B}_s]\,\mathrm{d}x$$

APPENDIX B: NOMENCLATURE

A	cross-sectional area of the flexible rod
$\mathbf{e}_\mathbf{i}$, $\mathbf{e}_\mathbf{j}$	unit vectors in the x' and y' directions, respectively
E	modulus of elasticity
G	shear modulus of elasticity
$\mathbf{i}$, $\mathbf{j}$	unit vectors in the X and Y directions, respectively
I	area moment of inertia about neutral axis
K	shape factor
L	length of the flexible rod
$l(t)$	element length
l_c	crank length
l_g	length of the ground link
M_c	mass of the crank
OXY	global co-ordinate system
$o'xy$	element co-ordinate system
$\mathbf{R}$	position vector of point P related to OXY co-ordinate system
$\mathbf{R}^\mathbf{i}$	position vector of point o' related to OXY co-ordinate system
$x_1'(t)$	current position of the translating/rotating joint
t	time
$u(x, t)$, $v(x, t)$	longitudinal and transverse displacements, respectively
$w(x, t)$	any unknown deformation
ϵ	dimensionless crank length parameter
θ	angle of the crank
ρ	mass density
Φ	angle of the undeformed axis of the flexible rod
ψ	rotation angle of the flexible rod
$\mathbf{\Omega}$	angular velocity of the crank